PCCP

RSC Publishing

PAPER

View Article Online
View Journal | View Issue

Cite this: *Phys. Chem. Chem. Phys.*, 2013, **15**, 11299

V^{5+} degradation of sulfonated Radel membranes for vanadium redox flow batteries†

Dongyang Chen and Michael A. Hickner*

Received 14th May 2013,
Accepted 23rd May 2013

DOI: 10.1039/c3cp52035h

www.rsc.org/pccp

Insight into the degradation mechanisms of aromatic proton conducting membrane separators for vanadium redox flow batteries (VRFBs) is urgently needed for the development of long lifetime VRFBs. Other than in-cell observations of performance degradation, there is little fundamental evidence on the specific degradation pathways of aromatic ion exchange membranes for VRFBs. Herein we investigated a sulfonated Radel® membrane (S-Radel) as the degradation target to study the degradation mechanism of aromatic polymers by V(v) (or generally V^{5+}) oxidation. It was found that the ductile S-Radel membrane, which has a similar aromatic backbone structure to the most-studied polyaromatic VRFB membranes that have shown high performance, became brittle and discolored after 3 days of immersion in 1.7 M V(v) + 3.3 M H_2SO_4 solution at 40 °C. The membrane's intrinsic viscosity was reduced to about half of its original value after this exposure to V(v) while the ion exchange capacity did not change. In addition to chain scission, it was found that –OH groups were introduced to the backbone of S-Radel as the major degradation product. Quinone groups were also observed at 1677 cm^{-1} in FTIR measurements. While the V(v) species in VRFBs is usually denoted as VO_2^+, V(v)═O in $VOCl_3$ was found to not have degradation activity for S-Radel. Therefore, we hypothesized that there were other reactive forms of V(v) species that first attacked the S-Radel by incorporating hydroxyl groups into the polymer's aromatic backbone, followed by the oxidation of these hydroxyl groups to quinone functionalities through a redox mechanism.

1. Introduction

Aqueous vanadium redox flow battery (VRFB) technology has emerged as one of the most promising technologies for large-scale energy storage because of its reliable operation without the risk of fire or explosion even at significantly high energy and power densities.[1,2] Key VRFB materials have received intense investigation over the last decade, which has lead to greatly improved cell performance. Over 95% coulombic efficiency (CE) and 80% energy efficiency (EE) can easily be achieved using carbon felt as the electrodes and an ion conductive membrane as the separator.[3,4] Dozens of demonstration programs have been implemented worldwide, with the highest power and capacity levels on the order of MW and MWh.[5] Currently, VRFB technology is considered one of the best on-site energy storage systems for large-scale solar and wind renewable power generation.[1]

While the optimized beginning of life cell performance is close to satisfying the needs for economical commercialization, long cycling performance and capacity maintenance of VRFBs are still critical challenges limited by the degradation of battery components such as the positive electrode and the electrolyte separator. It was found that the graphite plate, carbon cloth and carbon fiber underwent chemical and mechanical disintegration when used as the positive electrode of the VRFB.[6,7] The membrane separator also underwent breakage in long-term cell cycling and in *ex situ* immersion tests in the positive vanadium electrolyte containing V(v).[8,9] The strongly oxidative V(v) species in the positive electrolyte when the battery is in the charged state are usually considered to be responsible for degradation of the electrode and membrane components because V(iv) species (as the reduction product of V(v)) are generated accompanying degradation.[10] Additionally, immersion of membrane samples in V(iv) showed little to no degradation of a sulfonated aromatic membrane compared to significant degradation observed for immersion of the same sample in V(v).[8] Nevertheless, no detailed degradation mechanisms have been reported so far, which limits the design of long lifetime membranes for VRFBs.

Battery device cycling methods are the most direct but time-consuming method for membrane stability evaluations. In the

Department of Materials Science and Engineering, The Pennsylvania State University, University Park, PA 16802, USA. E-mail: hickner@matse.psu.edu; Fax: +1 814 865 2917; Tel: +1 814 867 1847

† Electronic supplementary information (ESI) available. See DOI: 10.1039/c3cp52035h

cell cycling test, the CE, EE or VE (voltage efficiency) generally remain unchanged or these cell metrics fluctuate around constant values until the membrane is compromised, where the CE, EE and VE drop sharply.[11,12] Under cell cycling, it is difficult to measure changes in membrane properties without conducting a number of experiments under different cycling conditions and then examining the membrane outside of the cell after test. The cycle number or cycling time can be used for stability comparisons of different membranes only if the cycling conditions are the same, such as the cycling current density and cell temperature. However, there is not an agreement on standard cycling conditions in the literature, which makes it difficult to rank the stability of different membranes for VRFBs from the reported data.[13–15] Fenton's reagent is another way to assess membrane stability, but it is not specific for VRFB operation because it only evaluates the general radical stability of the membranes instead of the oxidative stability from V(v) attack where redox processes are likely.[16,17] Therefore, evaluation of membranes by immersion in V(v)-containing electrolyte is the most efficient and effective way for membrane stability evaluations,[18,19] especially at elevated temperatures to accelerate degradation and shorten the experimental duration.[8] The drawback of this type of *ex situ* test is that the exact cell operation conditions are not replicated, so there may be degradation mechanisms occurring in the cell that are not captured. Thus, complementary immersion and in-cell cycling tests are needed, as we have demonstrated previously.[8]

By monitoring the weight loss of the membranes or the produced amount of V(IV) species during *ex situ* immersion in V(v)-containing electrolyte, it is possible to rank the relative stability of membranes.[20,21] However, no specific degradation mechanisms have been drawn from these measurements, which results in a lack of rational guidelines for next-generation membrane design for long lifetime VRFBs. We have developed several membranes for VRFBs using the state-of-art ion-exchange membrane structures, including sulfonated polysulfone (Radel®),[11] sulfonated poly(fluorenyl ether ketone),[18] sulfonated poly(arylene thioether)s,[22] and quaternary ammonium functionalized poly(fluorenyl ether).[23] None of these samples survived immersion in 1 M V(v) + 2 M H_2SO_4 solutions for 3 days at 40 °C while they all exhibited good cell performance at room temperature for at least 50 cycles and in some cases over 100 cycles in VRFBs. To provide more insight into the stability of ionic aromatic membrane separators for VRFBs, herein, we report our efforts to investigate the detailed physical and chemical changes of an archetypical sulfonated Radel membrane after V(v) degradation. Specific degradation pathways were then proposed, which are important for the future optimization of the material stability.

2. Experimental

2.1 Materials

Sulfonated Radel membrane (denoted as S-Radel, Scheme 1) with an ion exchange capacity of 1.4 mequiv. g^{-1} (water uptake = 20 mass%) was synthesized using a post-sulfonation scheme according to our previous report.[11] Membranes were cast from 8 wt/vol% DMAc solutions and dried at 80 °C under ambient pressure. V(v) electrolyte consisting of 1.7 M V(v) + 3.3 M H_2SO_4 was obtained by electro-oxidation of 1.7 M $VOSO_4$ + 3.3 M H_2SO_4 according to literature.[3] All other chemicals were purchased from common commercial suppliers and used as received.

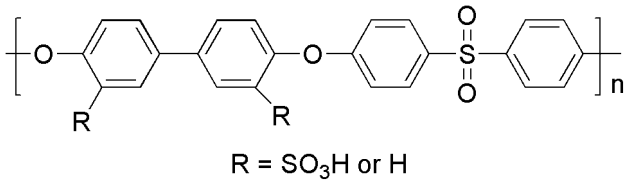

Scheme 1 Chemical structure of S-Radel membrane.

2.2 *Ex situ* degradation

0.2 g S-Radel membrane (~100 μm thick) was immersed in 50 mL V(v) electrolyte in a sealed glass vial. The vial was then conditioned at 40 °C in an oil bath for 72 h. After 72 h, the V(v) electrolyte was removed and the solid was rinsed with deionized water three times, followed by immersion in 50 mL 1 M H_2SO_4 solution for 24 h to protonate the sulfonate groups on the polymer and remove as much spurious vanadium species as possible. The H_2SO_4 solution was then replaced with deionized water to remove excessive acid from the membrane. A yellowish product of degraded S-Radel was obtained.

2.3 Characterization

Ion exchange capacity (IEC) was measured by titration. Dried membrane was weighed and immersed in a 1 M Na_2SO_4 solution for 24 h to deprotonate the sulfonic acid groups and form their sodium sulfonate salt. The resulting solution was titrated with a standardized 0.1 M KOH solution using phenolphthalein pH indicator. The intrinsic viscosities of S-Radel and degraded S-Radel were measured in 1-methyl-2-pyrrolidinone (NMP) containing 0.05 M LiBr at room temperature using a Ubbelohde viscometer. The thermal stability of the polymers was analyzed using a Q50 TGA (TA instruments Corp., USA). The temperature was increased from room temperature to 100 °C and held for 30 min, and then increased to 800 °C at a heating rate of 10 °C min^{-1} under argon atmosphere. Fourier transformed infrared spectroscopy (FTIR) spectra were recorded on a Bruker Vertex FTIR spectrometer. FTIR samples were prepared by casting a 3 wt% polymer *N*,*N*′-dimethylacetamide solution onto a CaF_2 crystal and then drying at 80 °C under ambient pressure for 24 h, followed by vacuum drying for 24 h. ^1H nuclear magnetic resonance (NMR) spectra were recorded on a Bruker AV-300 NMR instrument and the chemical shifts are listed in parts per million (ppm) downfield from tetramethylsilane (TMS). The mechanical properties were measured on an Instron 5866 Universal Testing Machine at room temperature. Scanning electron microscope (SEM) images were collected using a FEI Quanta 200 ESEM with an acceleration voltage of 20 kV. The cross-sections were obtained by cryo-fracturing samples in liquid nitrogen. SEM samples

were sputter-coated with gold prior to imaging. X-ray photoelectron spectroscopy (XPS) was measured on an ESCALAB 250 (Thermo-VG Scientific) analyzer under monochromatic Al (Kα) radiation (1486.6 eV, 15 kV and 150 W).

3. Results and discussion

The macroscopic and microscopic images of S-Radel and the degraded S-Radel samples are shown in Fig. 1. S-Radel was a transparent and dense membrane before degradation. After immersion in 1.7 M V(v) + 3.3 M H_2SO_4 at 40 °C, the membrane became yellow-colored and had brittle mechanical properties. Pores were formed throughout the membrane, as evidenced in the surface SEM image (Fig. 1(e)) and cross-section SEM image (Fig. 1(f)) of the degraded S-Radel sample. S-Radel is a typical aromatic cation exchange membrane that absorbs water to achieve high ion conductivity. The physical swelling of the material yields hydrophilic channels within the hydrophobic matrix, which are of crucial importance for cation conduction.[11] Since there are V(v) cations and protons in the electrolyte, some of the sulfonic acid sites in the hydrophilic channels of S-Radel are exchanged with V(v) cations while the diffusion of V(v) cations into the membrane is limited because of their larger ionic diameter as compared to the ionic diameter of the hydrated proton. This is similar to the cation exchange in V(IV) + H_2SO_4 electrolyte, where lower ionic conductivity was observed for the membrane because some of the proton sites were occupied by the low mobility V(IV) cations.[24,25] Therefore, because of significant V(v) uptake, degradation can happen throughout the membrane instead of occurring only at the outer surface of the sample. This type of degradation and access of V(v) to the internal structure of the membrane through the hydrophilic domains may explain the formation of the observed three dimensional pores in the degraded S-Radel.

The tensile properties of hydrated S-Radel and the degraded S-Radel samples are shown in Fig. 2. At low extension S-Radel underwent elastic deformation, reaching the yield strength of 14.1 MPa at the yield strain of 3.8%, and then plastic deformation occurred, in which the stress increased again with increasing strain until the specimen necked and fractured. The maximum tensile strength and elongation at break for S-Radel was 15.7 MPa and 49.2%, respectively. Therefore, S-Radel was initially ductile and displayed good mechanical attributes for VRFB operation. For the degraded S-Radel sample, only elastic deformation was observed in which the stress increased linearly with increasing strain until the specimen ruptured. The maximum tensile strength and elongation at break for degraded S-Radel were 12.8 MPa and 3.4%, respectively. According to the above SEM result, there were a lot of pores generated throughout the degraded S-Radel sample which would naturally weaken the sample and in this case cause brittleness.

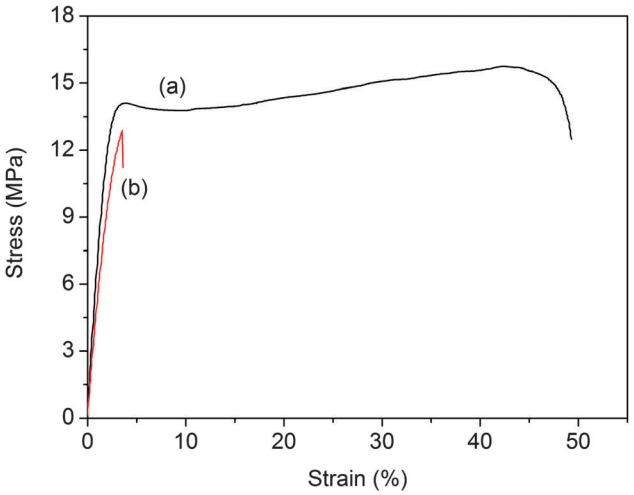

Fig. 2 Stress-strain curves of S-Radel and degraded S-Radel.

Both the SEM and tensile properties revealed that there was severe degradation during the 3 days' immersion test in 1.7 M V(v) + 3.3 M H_2SO_4 at 40 °C. The degraded S-Radel sample was

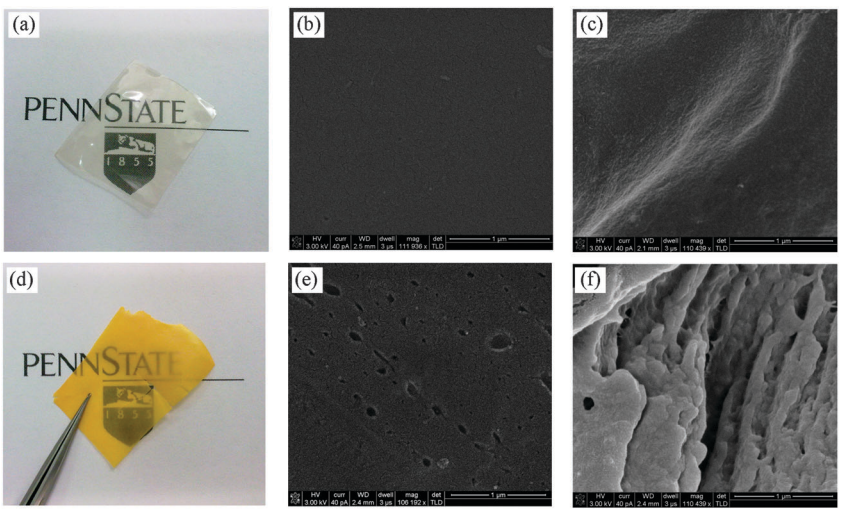

Fig. 1 S-Radel optical image (a), surface SEM image (b), cross-section SEM image (c) and degraded S-Radel optical image (d), surface SEM image (e), cross-section SEM image (f).

Table 1 Instrinsic viscosity and ion exchange capacity of S-Radel and degraded S-Radel

Sample	Instrinsic viscosity (dL g^{-1})	Ion exchange capacity (mequiv. g^{-1})
S-Radel	0.66	1.4
Degraded S-Radel	0.31	1.5

difficult to handle, as it broke easily upon physical bending and manipulation. In order to determine the specific degradation mechanisms during the immersion testing, we examined the relative molecular weight (represented by intrinsic viscosity) and IEC of S-Radel after degradation. The intrinsic viscosity was reduced from 0.66 dL g^{-1} to 0.31 dL g^{-1} for the degraded S-Radel while the IEC did not change much, as listed in Table 1. For a similar sulfonated poly(arylene ether sulfone) reported by McGrath *et al.*,[26] the decrease of intrinsic viscosity from 0.63 dL g^{-1} to 0.43 dL g^{-1} corresponded to a decrease of molecular weight from 38.1 kg mol^{-1} to 19.9 kg mol^{-1}. Drawing a parallel with the present work, we hypothesize that the molecular weight of S-Radel was reduced to less than half of its original value after degradation in V(v) solution. This result suggested that the polymer backbone underwent severe chain scission while the sulfonic acid groups remained nearly unchanged. This interesting observation prompted us to consider the intrinsic stability of the poly(arylene ether sulfone) structure under vanadium redox flow battery conditions and high V(v) concentrations. We immersed unfunctionalized Radel in the V(v) electrolyte, but no evidence of degradation was found even after two weeks due to the hydrophobicity of the unfunctionalized polymer and no access of water-soluble V(v) to the internal sample structure. Therefore, we can assert that intimate contact between the polymer chains and the V(v) species in a hydrophilic membrane is important for kicking off the degradation process.

In order to confirm the IEC observations from titration, thermogravimetric analysis (TGA) was applied to both S-Radel and the degraded S-Radel samples as shown in Fig. 3. Generally, the thermal decomposition of this type of ionomer has a two-step profile characteristic of the slow decomposition of sulfonic acid groups between 300 °C and 400 °C followed by rapid decomposition of the polymer backbone above 500 °C.[22] The weight change in the first step correlates to the IEC of the polymer. From Fig. 3 it can be seen that the TGA curves of S-Radel and degraded S-Radel almost overlapped, suggesting that the degradation did not influence the relative masses of sulfonate and backbone moieties.

The FTIR spectra of S-Radel and the degraded S-Radel samples are shown in Fig. 4. The asymmetric and symmetric stretching vibration peaks of the S=O bond in the sulfonic acid groups were found to be at 1025 cm^{-1} and 1093 cm^{-1} for S-Radel, while the symmetric stretching vibration peak was found at 1087 cm^{-1} and the asymmetric stretching vibration peak was likely merged into the adjacent peak at 1011 cm^{-1} for the degraded S-Radel. The peak intensities of sulfonic acid groups for the degraded S-Radel were reduced compared to

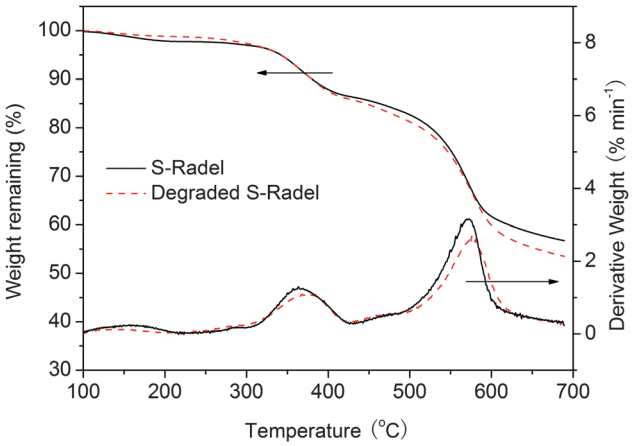

Fig. 3 TGA curves of S-Radel and degraded S-Radel.

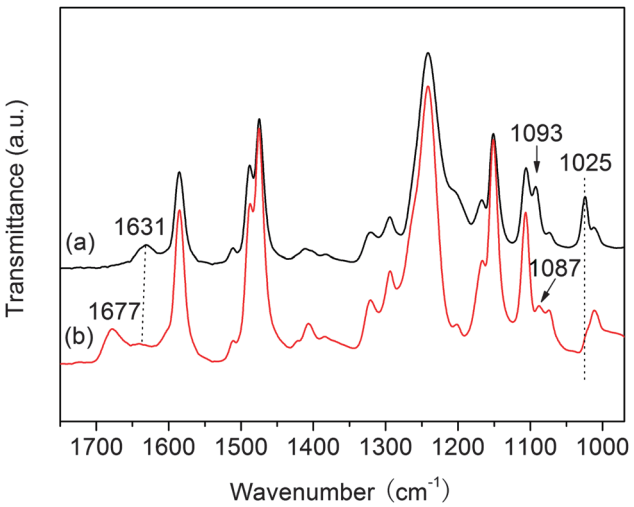

Fig. 4 FTIR spectra of S-Radel (a) and degraded S-Radel (b).

those in S-Radel. This change in the FTIR spectrum of the degraded sample suggested that the chemical environment of the sulfonic acid groups was altered after degradation if the concentration of sulfonic acid groups did not change per the TGA results. On the other hand, the bending vibration peak of O–H bond from the physisorbed water was found to be at 1631 cm^{-1} for S-Radel, but was shifted to 1642 cm^{-1} for the degraded S-Radel, implying that there was stronger hydrogen bonding after degradation. More interestingly, an obvious new peak was observed for the degraded S-Radel at 1677 cm^{-1}, which is in the range reported for quinone groups (1660–1680 cm^{-1}).[27] Since quinones are the oxidation products of phenols, there is a possibility that both of these moieties were the degradation products in our experiments. The full FTIR spectrum (Fig. S1 in ESI†) did not show any other drastic changes between fresh and degraded samples, ruling out the opening of phenyl rings to alkyl products.

XPS was used to indentify the elements and their valence states for S-Radel and degraded S-Radel samples. As shown in Fig. S2 (ESI†), only C, O and S elements were observed in the

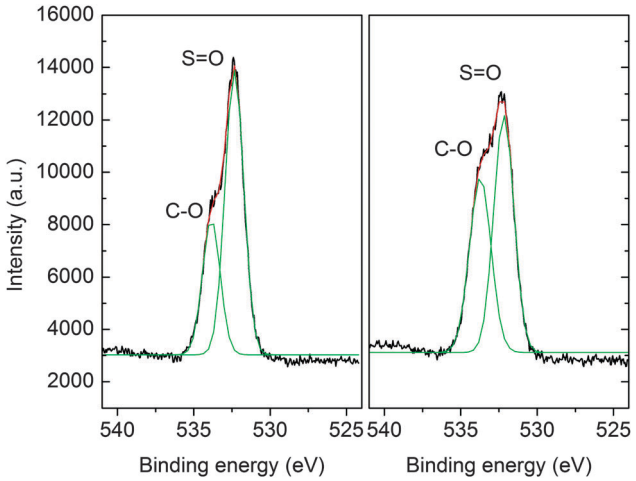

Fig. 5 XPS O1s spectra of S-Radel (left) and degraded S-Radel (right).

survey scan spectra. In the narrow scan spectra of O1s, Fig. 5, both samples exhibited a broad peak accompanied with a small shoulder peak, which was deconvoluted into two independent peaks corresponding to the two types of oxygen species in S-Radel, namely C–O (533.8 eV) and S═O (532.3 eV). After degradation, the C–O content obviously increased, as the peak intensity ratio of C–O to S═O increased from 0.46 for S-Radel to 0.79 for the degraded S-Radel. This result supported the observation that –OH groups were incorporated into S-Radel after degradation. While the FTIR spectrum of the degraded sample showed evidence of quinone moieties, the presence of quinone was unclear in the XPS results since the C═O peak may overlap with S═O peak and the concentration of quinone may be low. Because C═O has strong dipole moment, it usually has very strong absorption in FTIR even at relatively low concentration.

The XPS C1s spectra of S-Radel and degraded S-Radel were deconvoluted into four independent peaks, Fig. 6. These peaks corresponded to the four types of carbon species in S-Radel, which were C═C (284.8 eV), C–O (286.6 eV), C–SO_3H (289.2 eV) and C–SO_2–C (291.7 eV). After degradation, the peak intensity of C–O increased by 25%, further supporting the incorporation of –OH groups as degradation products. Another obvious change for the degraded S-Radel was that the peak intensity of C–SO_3H was reduced while the baseline was elevated. This observation may be attributed to the change of the electron density around the C–SO_3H carbon in the degraded S-Radel because of the –OH incorporation on the phenyl rings. In the event that –OH groups were oxidized to quinones, the C1s peak of the C═O groups would also fall in the region near the C1s peak of the C–SO_3H groups. The XPS S1s spectra for S-Radel and the degraded S-Radel were nearly identical except that the intensity of the S1s for the degraded S-Radel was slightly greater than that of S-Radel indicating that a slight increase in IEC might have occurred during aging in the H_2SO_4-based electrolyte.

^{1}H NMR and ^{13}C NMR spectroscopies were employed to investigate the chemical structures of S-Radel and the degraded S-Radel. The degraded S-Radel was found to be more soluble in common apotic solvents such as dimethyl sulfoxide (DMSO) and *N*,*N*′-dimethylacetamide (DMAc) than S-Radel. This increased solubility of the degraded sample supported the observation of the reduced molecular weight of the degraded S-Radel from IV measurements and also proved that cross-linking did not occur during the degradation process. After degradation, new aromatic protons peaks appeared at around 6.92 ppm and 7.81 ppm, Fig. 7. These new peaks had relatively low intensity. Due to the complexity of the possible degradation intermediates and products, it was very difficult to assign these peaks to specific proton-containing functional groups. The degraded samples did not have other detectable moieties like methyl or methylene since there was no other new proton signals in the full ^{1}H NMR spectrum of the degraded S-Radel as shown in Fig. S3 (ESI†). For the ^{13}C NMR spectra (Fig. S4, ESI†), no significant differences could be found between the fresh and degraded samples, suggesting that there was no detectable degradation product with distinctly new carbon moieties like carboxyl or aldehyde. This suggested again that if there were quinone degradation products, their content was low.

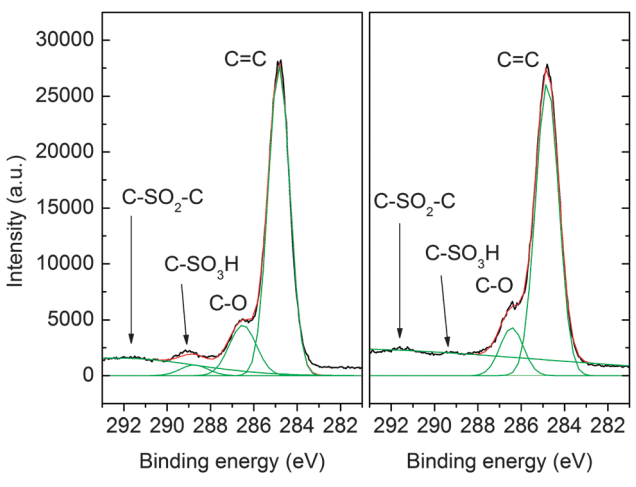

Fig. 6 XPS C1s spectra of S-Radel (left) and degraded S-Radel (right).

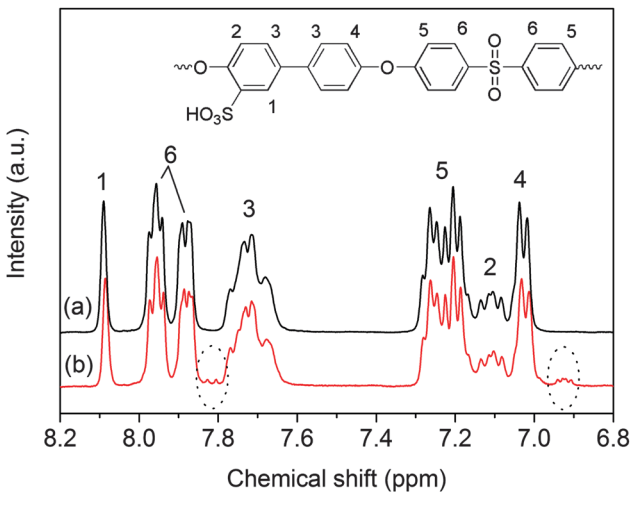

Fig. 7 ^{1}H NMR spectra of S-Radel (a) and degraded S-Radel (b) in DMSO-d_6.

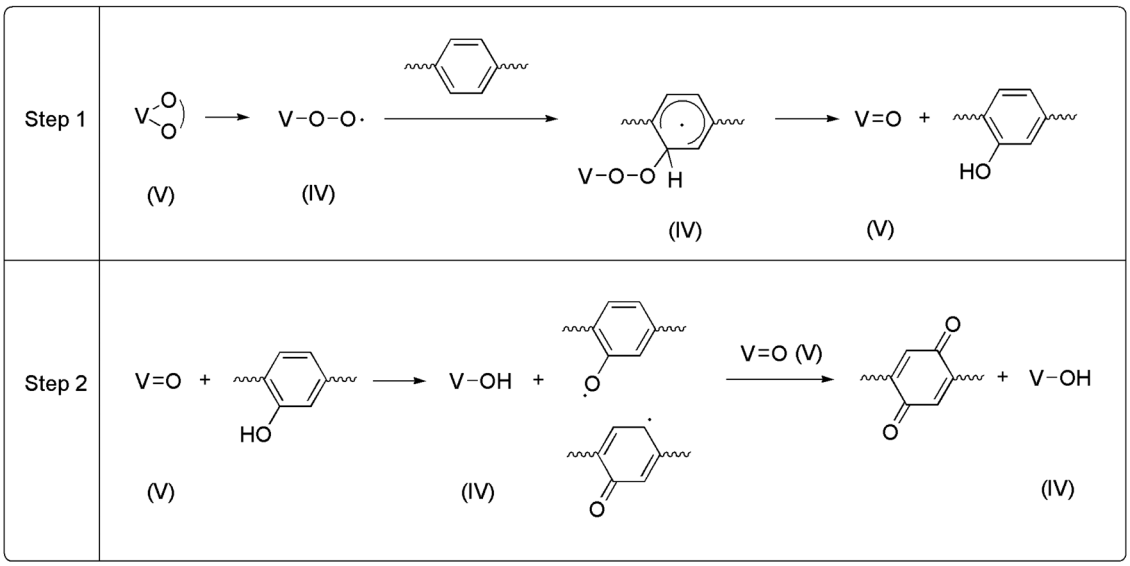

Fig. 8 Proposed degradation mechanism of S-Radel. Step 1 is a radical process while Step 2 is a redox process. Only the active parts of vanadium complexes are shown.

The V(v) species in the positive electrolyte of VRFBs are usually considered to be in the form of VO_2^+. However, we could not find literature precedent for the direct oxidation of an aromatic derivative by VO_2^+. In fact, we immersed our S-Radel membrane in neat $VOCl_3$ which contains V(v)═O similar to VO_2^+. No change in the S-Radel sample was observed in the experiment with $VOCl_3$. Thus, the VO_2^+ species is likely not the only species in the V(v) electrolyte as prepared by the electro-oxidation of VO^{2+}. There is also experimental evidence suggesting that the V(v) species in the positive electrolyte of VRFBs exist not only as VO_2^+, but also a number of other un-identified forms.[28] Interestingly, vanadium oxo peroxo complexes (V) are common and versatile reagents for the oxidation of benzene derivative to phenols. Vanadium oxo peroxo complexes such as $VO(O_2)(O–N)$ (N: pyridine-2-carboxylate) generate peroxo radicals easily that abstract hydrogen atoms from aromatic rings to give carbon radical intermediates.[29–31]

Based on the above observations, we propose the following degradation mechanism as shown in Fig. 8. The active forms of V(v) species (exampled by vanadium oxo peroxo complexes) generated vanadium peroxo radicals, which attacked the phenyl rings of the S-Radel leaving a phenol group on the polymer backbone while the vanadium species was converted into a less active V(v) species like VO_2^+. When the reaction took place at the phenyl–phenyl junctions, chain-scission occurred and the molecular weight or intrinsic viscosity of the polymer was decreased. At this point, the V(v) was not reduced to V(IV). However, we have observed a slight color change during the immersion test in this study and severe color changes in our previous long-term membrane assessments,[8] indicating the production of V(IV) during polymer degradation. Since VO_2^+ species are strong enough oxidizers to convert phenols to quinone,[32] we believe that the oxidation of the hydroxylated polymer backbone to quinone functionalities facilitated reduction of V(v) to V(IV). This assumption was in good accordance with our FTIR results. Limited by the concentration of hydroxyl groups on the polymer backbone, the content of quinone functionalities was too low to be detected in the NMR experiments. According to this mechanism, reducing the electron density of aromatic backbone with strategies such as fluorination or using hydrophobic phase separated structures that limit access of the degradative species to the polymer backbone may lower the risk of degradation for VRFB separators.

4. Conclusions

Sulfonated S-Radel membrane with an IEC of 1.4 mequiv. g^{-1} was degraded in a simulated positive VRFB electrolyte solution containing 1.7 M V(v) and 3.3 M H_2SO_4 at 40 °C for 3 days. The ductile S-Radel membrane became brittle after degradation. Three dimensional pores were formed throughout the membrane as observed by SEM. The intrinsic viscosity of the degraded S-Radel sample was only about half of that of the original S-Radel sample while the IECs were nearly equivalent. In the FTIR spectrum of the degraded S-Radel, the sulfonic acid peaks were affected and the O–H bend peak from the physisorbed water was shifted from 1631 cm^{-1} to 1642 cm^{-1}. A new peak at 1677 cm^{-1} was also observed, suggesting the generation of quinones after degradation. The XPS spectrum revealed more C–O bonds in the degraded samples in both the 1s O and C energy ranges. New small aromatic proton peaks in the ^1H NMR spectrum were observed for the degraded S-Radel while no other proton and carbon moieties were detected in the ^1H and ^{13}C NMR spectra. We hypothesized the degradation mechanism of S-Radel in the VRFB electrolyte had two steps. First, the active forms of V(v) species in the positive electrolyte of VRFB oxidized the phenyl rings of S-Radel by incorporating hydroxyl groups through a radical mechanism, which resulted in chain-scissioning of the S-Radel backbone. Since VO_2^+ is not active in this type of mechanism, the presence of vanadium oxo peroxides were surmised as the degradative species. Second, V(v) species

oxidized some of the hydroxylated polymer backbone into quinone functionalities through a redox mechanism, and green colored V(IV) species was produced.

Acknowledgements

The work was supported by the Office of Electricity (OE Delivery & Energy Reliability (OE), U.S. Department of Energy (DOE) under contract DE-AC05-76RL01830. We also acknowledge the support from the Southern Pennsylvania Ben Franklin Commercialization Institute (Grant #001389-002) and the Virginia S. and Philip L. Walker, Jr. Faculty Fellowship from the College of Earth and Mineral Sciences at The Pennsylvania State University.

References

1 G. Kear, A. A. Shah and F. C. Walsh, *Int. J. Energy Res.*, 2012, **36**, 1105–1120.
2 A. Parasuraman, T. M. Lim, C. Menictas and M. Skyllas-Kazacos, *Electrochim. Acta*, DOI: 10.1016/j.electacta.2012.09.067.
3 D. Chen, S. Kim, L. Li, G. Yang and M. A. Hickner, *RSC Adv.*, 2012, **2**, 8087–8094.
4 C. Fujimoto, S. Kim, R. Stains, X. Wei, L. Li and Z. G. Yang, *Electrochem. Commun.*, 2012, **20**, 48–51.
5 X. Li, H. Zhang, Z. Mai, H. Zhang and I. Vankelecom, *Energy Environ. Sci.*, 2011, **4**, 1147–1160.
6 M. Rychcik and M. Skyllas-Kazacos, *J. Power Sources*, 1987, **19**, 45–54.
7 H. Liu, Q. Xu, C. Yan and Y. Qiao, *Electrochim. Acta*, 2011, **56**, 8783–8790.
8 S. Kim, T. B. Tighe, B. Schwenzer, J. Yan, J. Zhang, J. Liu, Z. Yang and M. A. Hickner, *J. Appl. Electrochem.*, 2011, **41**, 1201–1213.
9 B. Schwenzer, J. Zhang, S. Kim, L. Li, J. Liu and Z. Yang, *ChemSusChem*, 2011, **4**, 1388–1406.
10 T. Sukkar and M. Skyllas-Kazacos, *J. Appl. Electrochem.*, 2004, **34**, 137–145.
11 S. Kim, J. Yan, B. Schwenzer, J. Zhang, L. Li, J. Liu, Z. Yang and M. A. Hickner, *Electrochem. Commun.*, 2010, **12**, 1650–1653.
12 D. Chen, S. Kim, V. Sprenkle and M. A. Hickner, *J. Power Sources*, 2013, **231**, 301–306.
13 Z. Mai, H. Zhang, X. Li, C. Bi and H. Dai, *J. Power Sources*, 2011, **196**, 482–487.
14 J. Xi, Z. Wu, X. Teng, Y. Zhao, L. Chen and X. Qiu, *J. Mater. Chem.*, 2008, **18**, 1232–1238.
15 H. Zhang, H. Zhang, F. Zhang, X. Li, Y. Li and I. Vankelecom, *Energy Environ. Sci.*, 2013, **6**, 776–781.
16 Y. Wang, J. Qiu, J. Peng, L. Xu, J. Li and M. Zhai, *J. Membr. Sci.*, 2011, **376**, 70–77.
17 D. Chen, S. Wang, M. Xiao, D. Han and Y. Meng, *Polymer*, 2011, **52**, 5312–5319.
18 D. Chen, S. Wang, M. Xiao and Y. Meng, *J. Power Sources*, 2010, **195**, 2089–2095.
19 J. Fang, H. Xu, X. Wei, M. Guo, X. Lu, C. Lan, Y. Zhang, Y. Liu and T. Peng, *Polym. Adv. Technol.*, 2013, **24**, 168–173.
20 N. Wang, S. Peng, H. Wang, Y. Li, S. Liu and Y. Liu, *Electrochem. Commun.*, 2012, **17**, 30–33.
21 B. Tian, C. W. Yan and F. H. Wang, *J. Appl. Electrochem.*, 2004, **34**, 1205–1210.
22 D. Chen, S. Wang, M. Xiao and Y. Meng, *Energy Environ. Sci.*, 2010, **3**, 622–628.
23 D. Chen, M. A. Hickner, S. Wang, J. Pan, M. Xiao and Y. Meng, *Int. J. Hydrogen Energy*, 2012, **37**, 16168–16176.
24 D. Chen, M. A. Hickner, E. Agar and E. C. Kumbur, *Electrochem. Commun.*, 2013, **26**, 37–40.
25 Z. Tang, R. Keith, D. S. Aaron, J. S. Lawton, A. P. Papandrew and T. A. Zawodzinski, *ECS Trans.*, 2012, **41**, 25–34.
26 Y. Li, F. Wang, J. Yang, D. Liu, A. Roy, S. Case, J. Lesko and J. E. McGrath, *Polymer*, 2006, **47**, 4210–4217.
27 M. Buschel, C. Stadler, C. Lambert, M. Beck and J. Daub, *J. Electroanal. Chem.*, 2000, **484**, 24–32.
28 E. Wiedemann, A. Heintz and R. N. Lichtenthaler, *J. Membr. Sci.*, 1998, **141**, 207–213.
29 H. Mimoun, L. Saussine, E. Daire, M. Postel, J. Fischer and R. Weiss, *J. Am. Chem. Soc.*, 1983, **105**, 3101–3110.
30 G. B. Shulpin, D. Attanasio and L. Suber, *J. Catal.*, 1993, **142**, 147–152.
31 T. K. Si, K. Chowdhury, M. Mukherjee, D. C. Bera and R. Bhattacharyya, *J. Mol. Catal. A: Chem.*, 2004, **219**, 241–247.
32 P. N. Remya, C. H. Suresh and M. L. P. Reddy, *Polyhedron*, 2007, **26**, 5016–5022.